BRL

REPORT NO. 1333

INTERFEROMETRIC MEASUREMENT OF THE NONEQUILIBRIUM FLOW FIELD AROUND A CONE

by

J.H. Spurk
J.M. Bartos

August 1966

B A L L I S T I C   R E S E A R C H   L A B O R A T O R I E S

REPORT NO.   1333

AUGUST 1966

Distribution of this document is unlimited.

INTERFEROMETRIC MEASUREMENT OF THE NONEQUILIBRIUM
FLOW FIELD AROUND A CONE

J. H. Spurk
J. M. Bartos

Exterior Ballistics Laboratory

RDT&E Project No. 1P222901A201

A B E R D E E N   P R O V I N G   G R O U N D ,   M A R Y L A N D

B A L L I S T I C   R E S E A R C H   L A B O R A T O R I E S

REPORT NO. 1333

INTERFEROMETRIC MEASUREMENT OF THE NONEQUILIBRIUM
FLOW FIELD AROUND A CONE

ABSTRACT

Interferometric measurement of the density field around a cone in a stream of oxygen at approximately 10,000 ft/sec is reported. The test flow was generated in an expansion tube, which utilized an unsteady expansion for the purpose of total enthalpy multiplication. The experiment shows that vibrational equilibrium is achieved close behind the shock, while chemical relaxation occurs throughout the shock layer. The experimental density distribution and shock shape are compared with theoretical predictions, and good agreement is found.

TABLE OF CONTENTS

BLANK PAGE

I. INTRODUCTION

The large number of numerical and analytical studies in nonequilibrium flow fields around bodies is not accompanied by an equally large amount of experimental studies. Actually, experimental data for nonequilibrium flows is extremely scarce. The main reason appears to be the difficulty in generating a high Mach number test flow of gas in a known thermodynamic state and with sufficient total enthalpy. The necessarily short testing times of ground facilities operating at extreme enthalpy levels and the large number of variables in nonequilibrium flow further complicate the experiments. However, it has been recognized that, by virtue of enthalpy multiplication in an unsteady expansion, test flows with high enthalpy and low free stream dissociation levels can be obtained. Several operation cycles of recently proposed hypervelocity facilities incorporate such an unsteady expansion.[1-3*] Instrumentation techniques with sufficiently short response time have been developed for use in these facilities. In particular the optical interferometer, which allows an unperturbed observation of the flow, is a very attractive diagnostic tool in studying short duration high enthalpy flows.

This report describes the interferometric measurement of the density field around a cone in a stream of oxygen at approximately 10,000 ft/sec. The test flow was generated in an expansion tube which employs an unsteady expansion for the purpose of total enthalpy multiplication.

II. EXPERIMENTAL TECHNIQUE

In this section the facility and the experimental setup will be described as far as needed for the understanding and critique of the experiment. A more detailed description may be found in References 4 and 5. Figure 1, an x, t diagram, shows the operation cycle of an expansion tube. A thorough theoretical study of an expansion tube facility is reported in Reference 1. Referring to Figure 1, we note that an observer at station x_o sees first the passage of a shock, followed by a region of constant flow properties. This region 20 can be used for testing, but is not of

---

Superscript numbers denote references which may be found on page 30.
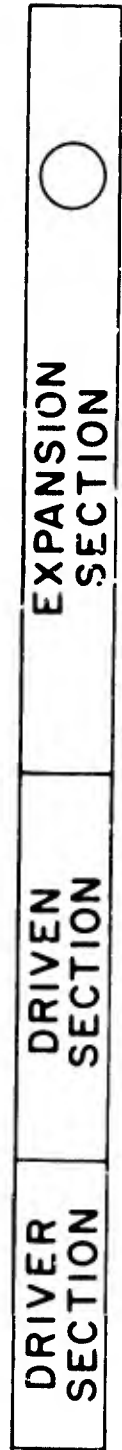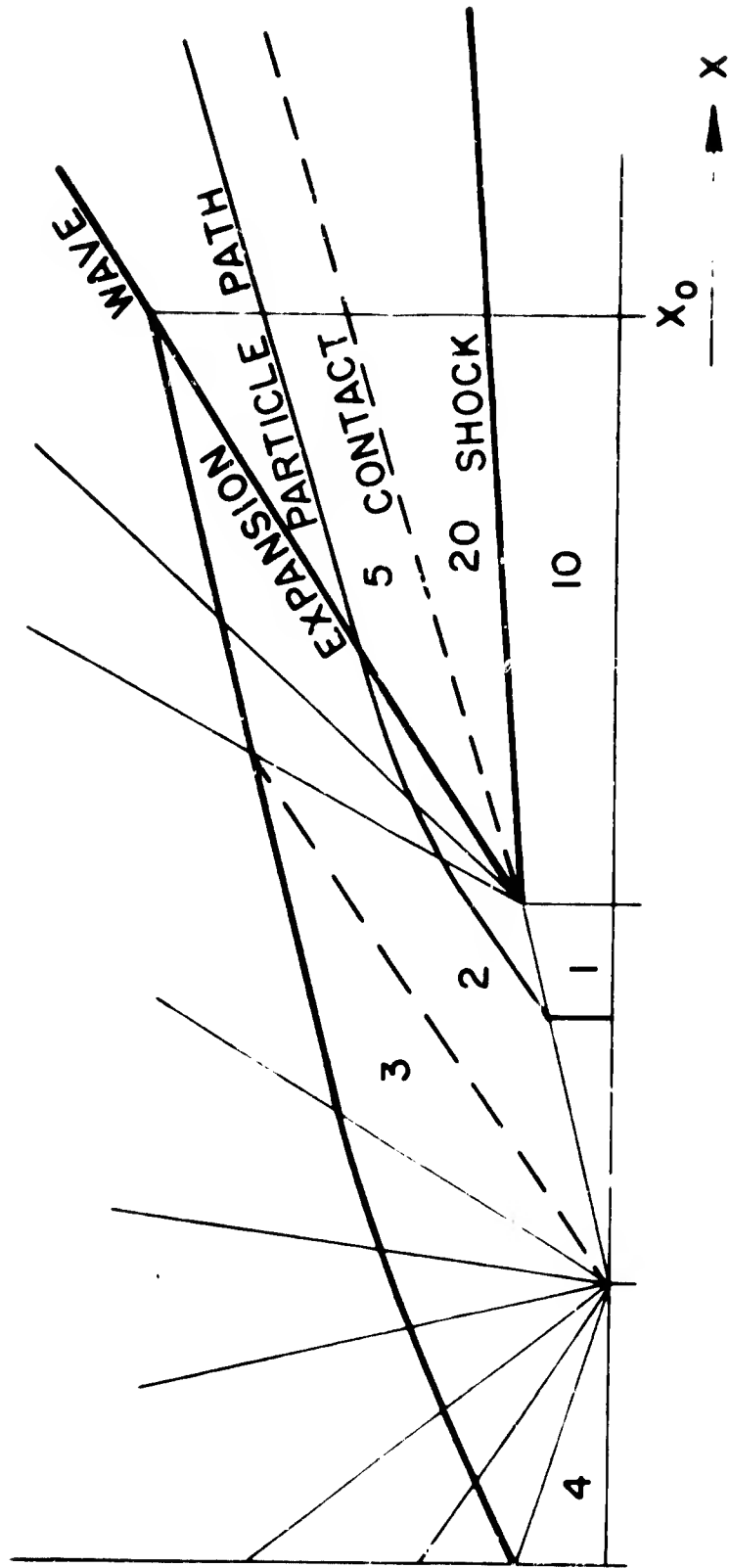
7

Figure 1. Expansion Tube Cycle

interest here. Next, one observes the passage of the contact front, followed by another region 5 of constant flow properties. This is the test region; it constitutes a region of high enthalpy, high Mach number flow in contrast to region 2 where the Mach number is low and limited.

Recently there has been an account of experimental investigations of expansion tubes.[5-8] While some experimenters report considerable disturbances in the test flow for test times of about 500 μsec, all reports indicate fairly constant flow conditions for test times of 50 to 100 μsec after passage of the contact front. It appears that diaphragm contamination will not be a severe problem (except possibly for radiation studies), and conical flow tests indicate surprisingly low free stream turbulence.

The expansion tube used in this experiment consists of essentially three sections: driver, driven and expansion sections, see Figure 1. The expansion section, the major component of the facility is 35 ft long with an I.D. of 7.25 inches. A 6.42-in. square cross-section is attached to the expansion section. Circular windows, four inches in diameter, in the sidewall allow observation of the flow through a 10-in. Mach-Zehnder interferometer. By means of streak interferometry the flow conditions in the free stream over a period of 300 μsec from the arrival of the shock at the test station are recorded. The streak is obtained by observing the flow through slits and sweeping the image on a film drum. The frame interferogram is taken 80 μsec after passage of the contact front at the test station. An example of a streak interferogram can be found in Reference 4; the frame interferogram is reproduced in Figure 2.

Shock mounted pressure gages in the test section are used to measure static pressure and shock speed. The static pressure was 0.34×10^5 dyn/cm^2 and constant for 300 μsec after shock arrival. The shock speed was 3450 m/sec.

The oxygen used was commercial oxygen, 99.6 percent pure. No greater care was warranted since some contamination by diaphragm particles was anticipated. It is known that impurities are usually less efficient in producing dissociation than the dissociating gas itself.[9] A small amount of impurity will not appreciably change the reaction rate.

9

Figure 2. Frame Interferogram of the Flow Field Around the Model. u_∞ = 3450 [m/sec], M_∞ = 8.71 ρ_∞ = 0.0337 [kg/m^3]

Oxygen at 7 psia was admitted into the evacuated driven section prior to the test run. Initially the driver section was filled with helium at 3600 psia and the expansion section with air at 200 μ Hg.

A cone cylinder 1.5 ±0.001 in. diameter and 54.0 ±0.05 degrees half angle with a precision ground finish served as the model.

III. THE REDUCTION PROCESS

The quantity measured in the interferogram is the fringe shift δ, which is the change of fringe position between the undisturbed reference pattern and the disturbed pattern in units of undisturbed fringe spacing. The undisturbed fringe pattern is extrapolated over the disturbed region. The fringe shift is caused by the change in the index of refraction and is given by:

$$\delta(x,r) = \frac{1}{\lambda} \int (\mu - \mu_{ref}) ds \qquad (1)$$

where s is the light path, λ the observing wave length, μ the index of refraction and x,r coordinates normal to s. The Gladstone-Dale relation determines the density of a dilute gas if the refractivity K is known

$$\mu - 1 = K\rho . \qquad (2)$$

K can be calculated for a gas consisting of different species "i"

$$K = \sum K_i \rho_i / \rho \qquad (3)$$

if the partial densities ρ_i of the gas components and their specific refractivities K_i are known.

In the present experiment the test gas is expanded from an undissociated state (region 2 of Figure 1) so that it is in chemical equilibrium. Vibrational nonequilibrium can be expected, however. From (1), (2) and (3) there follows for the density in the free stream

$$\rho_\infty(x,r) = \frac{\lambda \delta(x,r)}{SK_\infty} + \rho_{ref} \qquad (4)$$

11

with S being the width of the test section. Under these conditions the free stream temperature is $T_\infty = P_\infty / \rho_\infty R$ where p_∞ is the static pressure measured in the test section.

In order to evaluate the axisymmetric flow around the model, (1) is rewritten as [10,11]

$$\delta(x,r) = \frac{2}{\lambda} \int_r^{r_s} \frac{(\mu - \mu_\infty) r' dr'}{(r'^2 - r^2)^{1/2}} \qquad (5)$$

r_s in this case is the shock radius, x,r are the coordinates of the point for which δ is given by (5), and r' is an inner point. (5) may be solved to give the change in index of refraction

$$\mu(x,r) - \mu_\infty(x,r) = \frac{-\lambda}{\pi} \int_r^{r_s} \frac{\frac{d\delta}{dr'}}{(r'^2 - r^2)^{1/2}} dr' \qquad (6)$$

Reduction of (6) to give the density field of a partially dissociated gas will require the knowledge of the specific refractivities K_i and the partial densities ρ_i of the species present. Even if the specific refractivities are known, the reduction to density can in general not be accomplished for nonequilibrium flows, since the partial densities are not known.

The specific refractivities of gases at high temperatures are not well known; for the atomic constituents of high temperature air, the refractivities have been measured by Alpher and White.[12] The specific refractivities of the molecular species at room temperature are probably valid for higher temperatures also, because the effects of vibrational and electronic excitation of the diatomic molecules on the refractive index is thought to be negligible. Recent work,[13] however, indicates that there is an effect, and the refractivity for molecular oxygen K_{O_2} is about five percent higher in the temperature range of the interest here than at room temperature. Fortunately, the interferometric measurement of the density is still possible, since the overall refractivity $K = \sum K_i \rho_i / \rho$ is almost constant in the shock layer for many cases of

practical interest. For the conditions of this experiment numerical com-
putations of the nonequilibrium flow and subsequent calculation of K show
this quantity to vary less than one percent in the shock layer.

Similar computations for nonequilibrium airflows with considerably
higher free stream velocities show K again to be almost constant in the
shock layer. Since the specific refractivity of molecular oxygen is
almost that of atomic oxygen and the specific refractivity of nitric
oxide that of undissociated air[12] the assumption of constant $K \sim K_{Air}$ is
justified as long as nitrogen dissociation is small. The atomic nitrogen
concentration in the shock layer of a nonequilibrium flow is lower and
the assumption of constant K is better than for equilibrium flow.

Assuming K to be constant, $K \sim K_\infty$, the density field is determined by

$$\rho(x,r) - \rho_\infty = \frac{-\lambda}{\pi K_\infty} \int_r^{r_s} \frac{\frac{d\delta}{dr'} dr'}{(r'^2 - r^2)^{1/2}} \quad . \tag{7}$$

This integral (7) can be evaluated numerically for fringe shift values
$\delta = f(r)$ at traces x = constant. The evaluation requires a smooth curve
to be drawn through the data points δ versus r. If the density distribu-
tion displays a discontinuity, for example at the shock, the use of
"reduced" fringe shift is better suited:

$$\delta_{red} = \delta - \frac{2K_\infty \bar{\rho}}{\lambda} (r_s^2 - r^2)^{1/2} \tag{8}$$

giving:

$$(\rho - \rho_\infty)_{red} = (\rho - \rho_\infty) - \bar{\rho} \tag{9}$$

$\bar{\rho}$ is the step discontinuity at the shock. For improper choice of the
deshocking constant, $\bar{\rho}$, spurious density values near the shock may re-
sult which, however, die out rapidly. Besides the zone close to the
shock, error accumulation in the reduction process is only appreciable as
r approaches zero.[10] This region is avoided in the present study.

IV. MEASUREMENT OF THE INTERFEROGRAMS

The fringe shift is measured as the difference of ordinates of the undisturbed fringe position and the disturbed fringe position in a suitable reference coordinate system. The undisturbed fringe location is found by linearly extrapolating the undisturbed fringes ahead of the disturbance into the disturbed field. In practice this amounts to measuring the ordinates of the undisturbed fringes at a reference station, the inclination of the fringes to the reference coordinate system, and the ordinates of corresponding fringes at the trace x = constant.

The streak interferogram (with x coordinate as the time) was measured on a film reader. The undisturbed fringes were aligned parallel to the abscissa of the film reader coordinate system by means of a reference line put on the streak during exposure of the film. The accuracy of the measurement was at best ten percent of the fringe spacing, due to the particular film format of the streak, which allows only a small magnification in the readout instrument. The fringe shift, $\delta \sim 1.5$, is constant in time within ten percent for about 80 µsec, indicating constant free stream conditions. Figure 3 shows the fringe shift across the field of view at the instant the frame picture was taken. The scatter gives an indication of the accuracy of the measurement; however, apart from scatter there is a variation of fringe shift (density) across the field of view of about plus or minus ten percent.

The frame interferogram was measured on a stereo-comparator with plus or minus one percent absolute accuracy. The interferogram is adjusted, using the body contour of the model. The apex of the cone could be located within 20 µ (two percent of the fringe spacing), and the misalignment between the axis of the cone and the reference coordinate system is less than 0.2 degree. The shock position was measured first and was found to be symmetric within the measuring accuracy. Measurement of the fringe shift was performed at 10 traces (x = constant) in an interval 5mm < x < 12mm. For traces at x less than 5mm only a fringe shift of 1 occurs, with very few data points in the shock layer. The fringe position
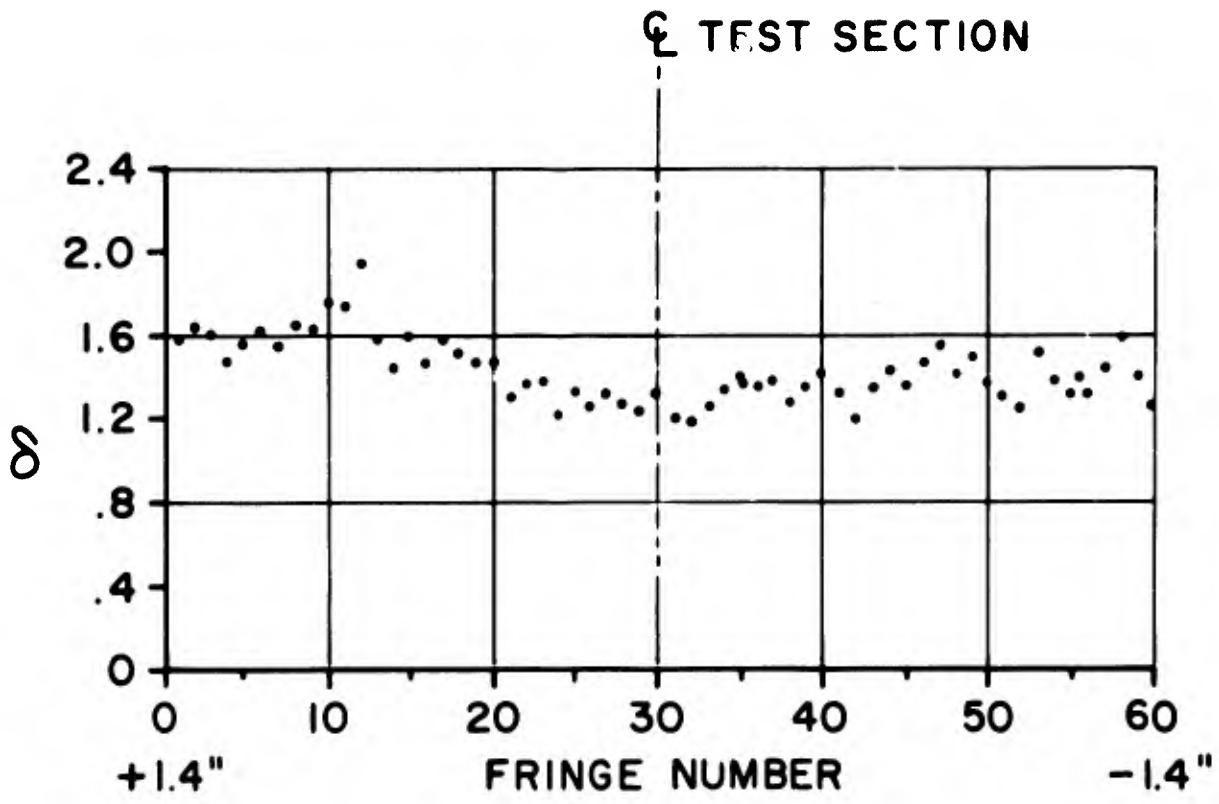
14

Figure 3.   Variation of the Fringe Shift δ Across the Field of
            View

was averaged over four readings. Successive readings made by the same observer were reproducible to 2.5 percent of the fringe spacing. These readings are not influenced by the boundary layer at the walls. A maximum error of three percent is introduced by extrapolating the undisturbed fringes into the disturbed region, because the undisturbed fringes are not quite parallel and are slightly curved. This is most likely an indication of a small disturbance in the flow, but there is a possibility that it is caused by a faulty mirror coating. (The coating was being attacked by fumes of a cleaning agent used in cleansing the tube; the damage was not noticed at the time of this experiment.)

The fringe shift at different trace positions has also been measured by following one fringe through the disturbance rather than measuring the position of different fringes at one trace position. This method is more time-consuming, but a somewhat higher accuracy can be achieved. The accuracy of the fringe shift measurement is not uniform over the field, but it is believed that it is five percent or better over most of the field.

V. OUTLINE OF NONEQUILIBRIUM FLOW CALCULATION

To provide theoretical data for comparison with experiment, the inviscid, non-heatconducting flow over the cone has been computed. The oxygen is considered to consist of two neutral species, atoms and diatomic molecules. In the temperature range considered here, triatomic oxygen molecules play no role. The mixture is assumed to be in translational, rotational and vibrational equilibrium at all times; the only nonequilibrium processes are chemical reactions. Each species shall have perfect gas properties; its internal energy shall have contributions from translation, rotating and vibration only. The hyperbolic system of fluid dynamic and chemical reaction rate equations can be reduced to a system of ordinary differential equations by introduction of characteristic directions. This system is numerically integrated, starting from a region of chemically frozen flow at the tip of the body. A detailed description of the computations can be found in Reference 14.

The chemical reactions occurring in this flow are represented as:

$$O_2 + O_2 \rightleftarrows 2O + O_2 \qquad\qquad (10)$$

$$O_2 + O \rightleftarrows 3O$$

These reactions have been investigated by several workers. For the temperature range of interest here, reaction rate coefficients have been given for O_2 as catalytic species by Byron[15] and Mathews[9] and for O as a catalytic species by Byron.[15] Somewhat different coefficients are employed in the numerical computations of Reference 16, but they are based on data from Byron. The rate coefficients k_{O_2} are shown in Figure 4 for comparison. The effect of these different rate coefficients on density and species concentration is worth noting. Figure 5 shows the dependence of these quantities through the shock layer at a trace x = 4.92mm for typical free stream conditions. All other theoretical computations are based on rate coefficients and equilibrium constants as used in Reference 16.

VI. DISCUSSION OF EXPERIMENTAL RESULTS AND COMPARISON WITH CHARACTERISTIC COMPUTATIONS

Considering first the free stream conditions, it is noted that free stream density is the most uncertain quantity in this experiment. Application of (4) presupposes the density to be constant along s, the light path. Actually, the density varies considerably. First, the density varies through the boundary layer on the windows. This variation can be estimated assuming ideal gas and flat plate steady boundary layer, and indicates that ρ_∞ should be increased 17 percent over the value from (4). Secondly, as suggested by Figure 3, the density is expected to vary in the s direction outside the boundary layer. This density variation is not known, of course; possibly it has only a small effect on the average density ρ_∞ .

The free stream density, $\rho_\infty = 0.0337$ kg/m^3, accepted for most of the theoretical calculations, is determined from the fringe shift at the centerline of the test section (Figure 3), according to (4), and tentatively increased 15 percent to account for boundary layer effects.
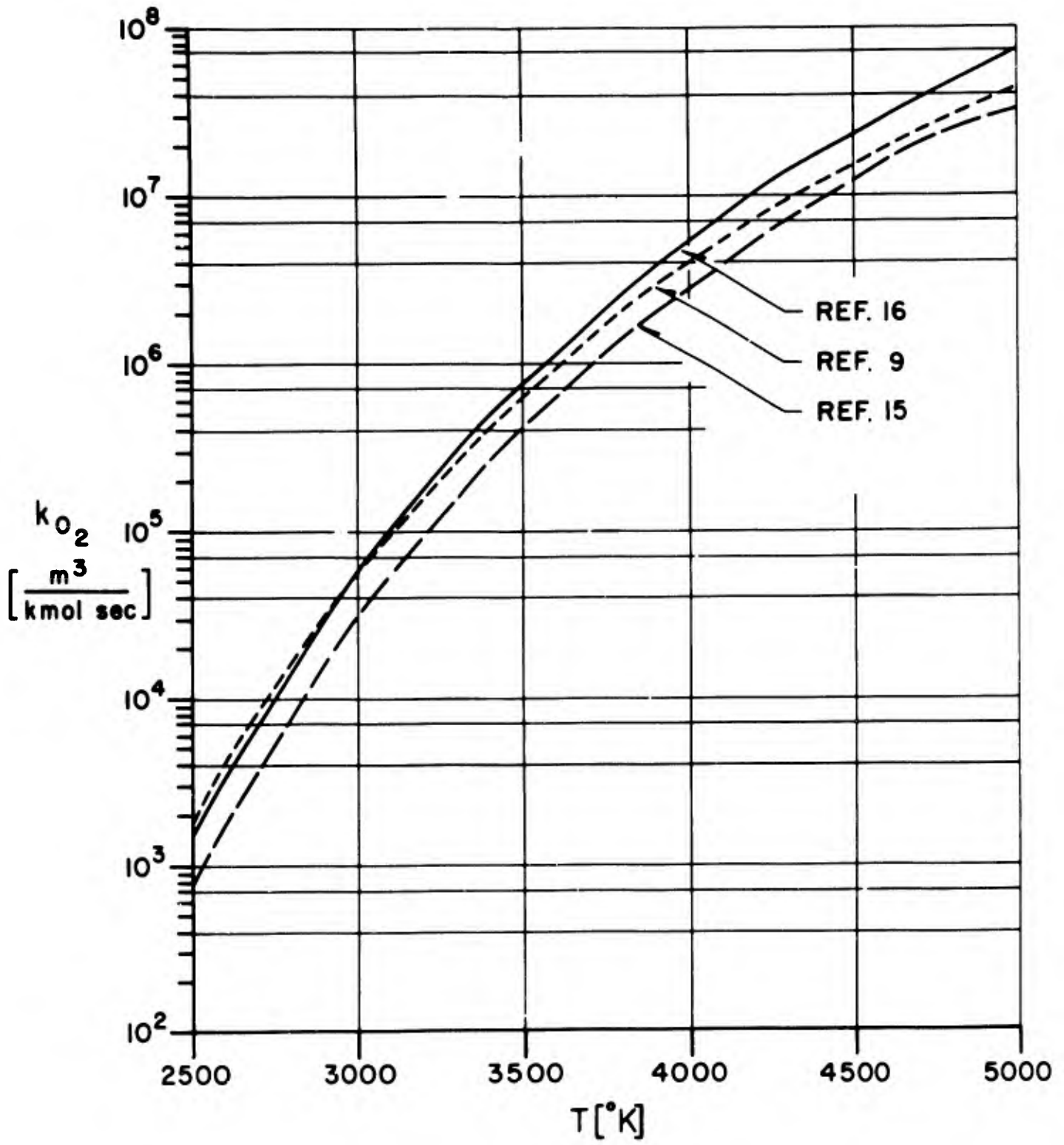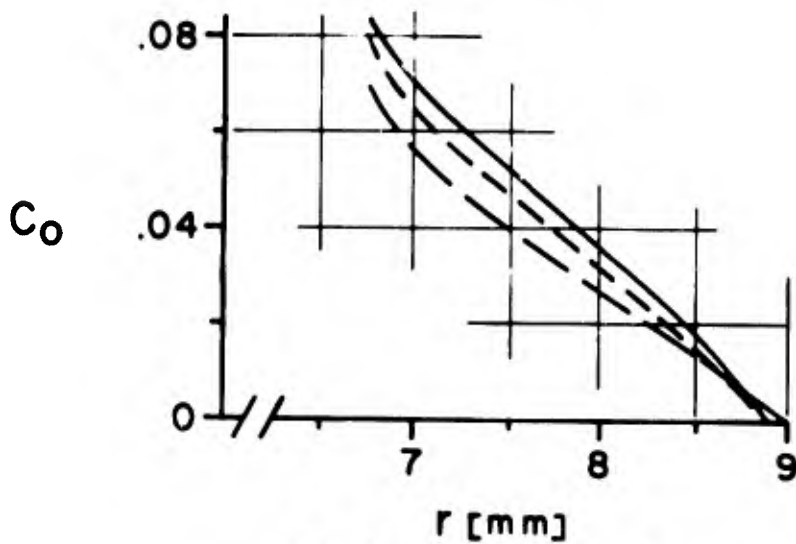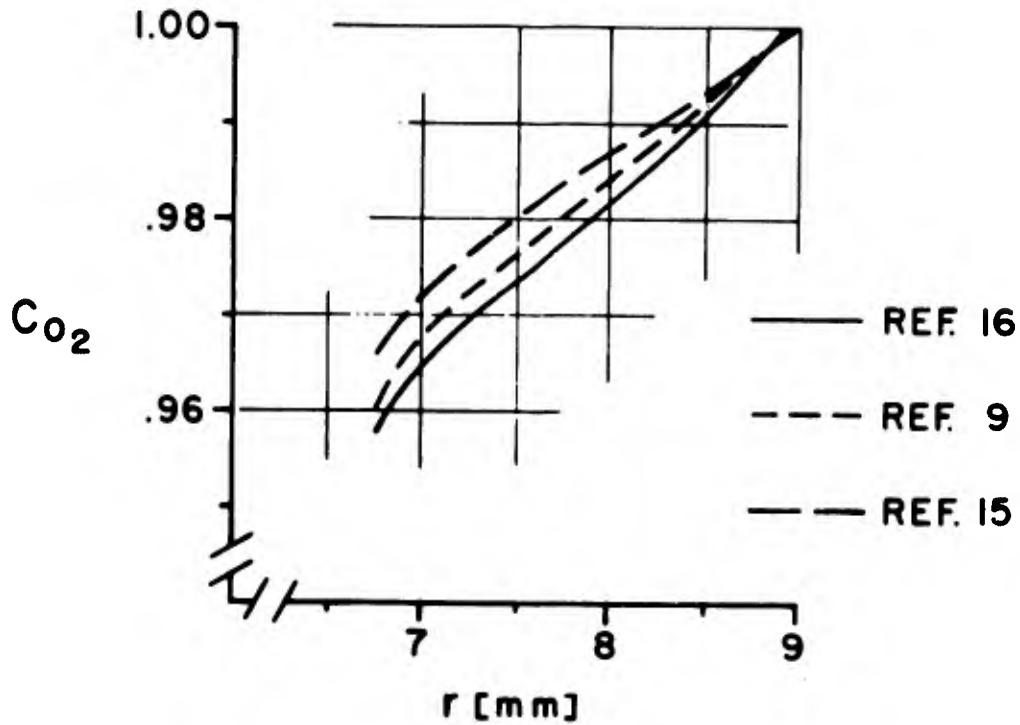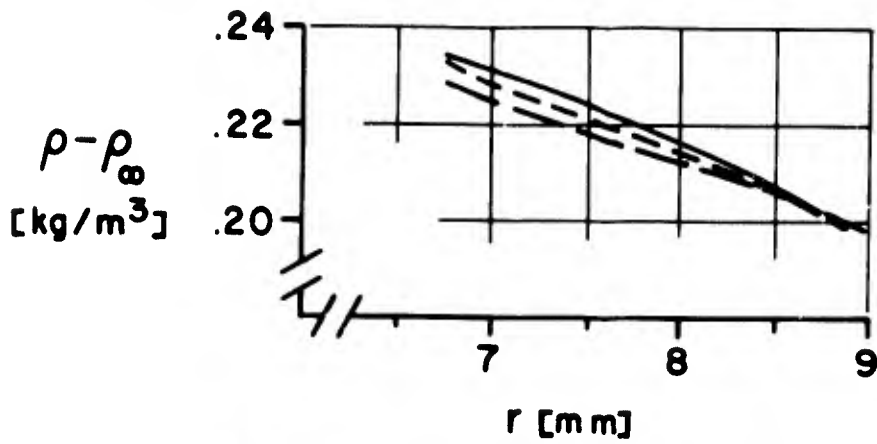
Figure 4. Comparison of Dissociation Rate Coefficient for O_2 From Different
Sources   18

Figure 5. Theoretical Density and Species Concentration Distributions, $\rho - \rho_\infty$, c_0, c_{0_2} versus r, Across the Shock Layer for the Different Values of Rate Coefficient of Figure 4.

In order to have a notion of the effect of uncertainty in free stream density, inspect Figure 6, which shows the density difference $\rho - \rho_\infty$ in the shock layer at a trace $x = 8.56$mm computed for different values of free stream density; these are based on the density, according to (4), plus an increase of 10, 15, and 20 percent respectively. Figure 6 also displays the effect of a parametric change of the free stream velocity. The free stream velocity is assumed to be equal to the contact front velocity which, for the conditions considered, is essentially equal to the shock velocity[17] ($u_s = 3450 \pm 100$ m/sec). No parametric variation of the free stream pressure has been done (the experimental pressure deviates 6 percent from the pressure based on shock velocity $u_s = 3450$ m/sec). Change in free stream pressure will only influence the temperature T_∞, and thus the enthalpy h_∞, which is very small compared to the total enthalpy. The net effect of pressure variation on density distribution and shock geometry will therefore be small indeed.

The theoretical calculations are based on the following free stream values: $\rho_\infty = 0.0337$ kg/m^3, $T_\infty = 388.5°$K, $p_\infty = 0.34 \times 10^5$ dyn/cm^2, $u_\infty = 3500$ m/sec. Inspection of Figures 6-8 and other data reveal that the best overall agreement between prediction and experiment will exist for density values ρ_∞ in the range 0.0337 to 0.035 kg/m^3 and velocities u_∞ between 3400 and 3500 m/sec.

Most of the experimental results are shown in the form $\rho - \rho_\infty$ versus r, as obtained from the frame interferogram alone through (7). The density difference $\rho - \rho_\infty$ is independent of ρ_∞, and ambiguity resulting from uncertain value of ρ_∞ is avoided. Results in the dimensionless form ρ/ρ_∞ are based on the free stream value $\rho_\infty = 0.0337$ kg/m^3.

Before turning to the density distribution across the shock layer, mention will be made of the arbitrariness introduced by the graphical smoothing of the measured fringe shift data. Figure 7 shows the effect on density distributions of two different, but possible, smooth curves drawn through the data points. Shown also is the density distribution obtained by immediate use of the data points. As expected, this leads to fluctuations in the density distribution which, however, bracket the
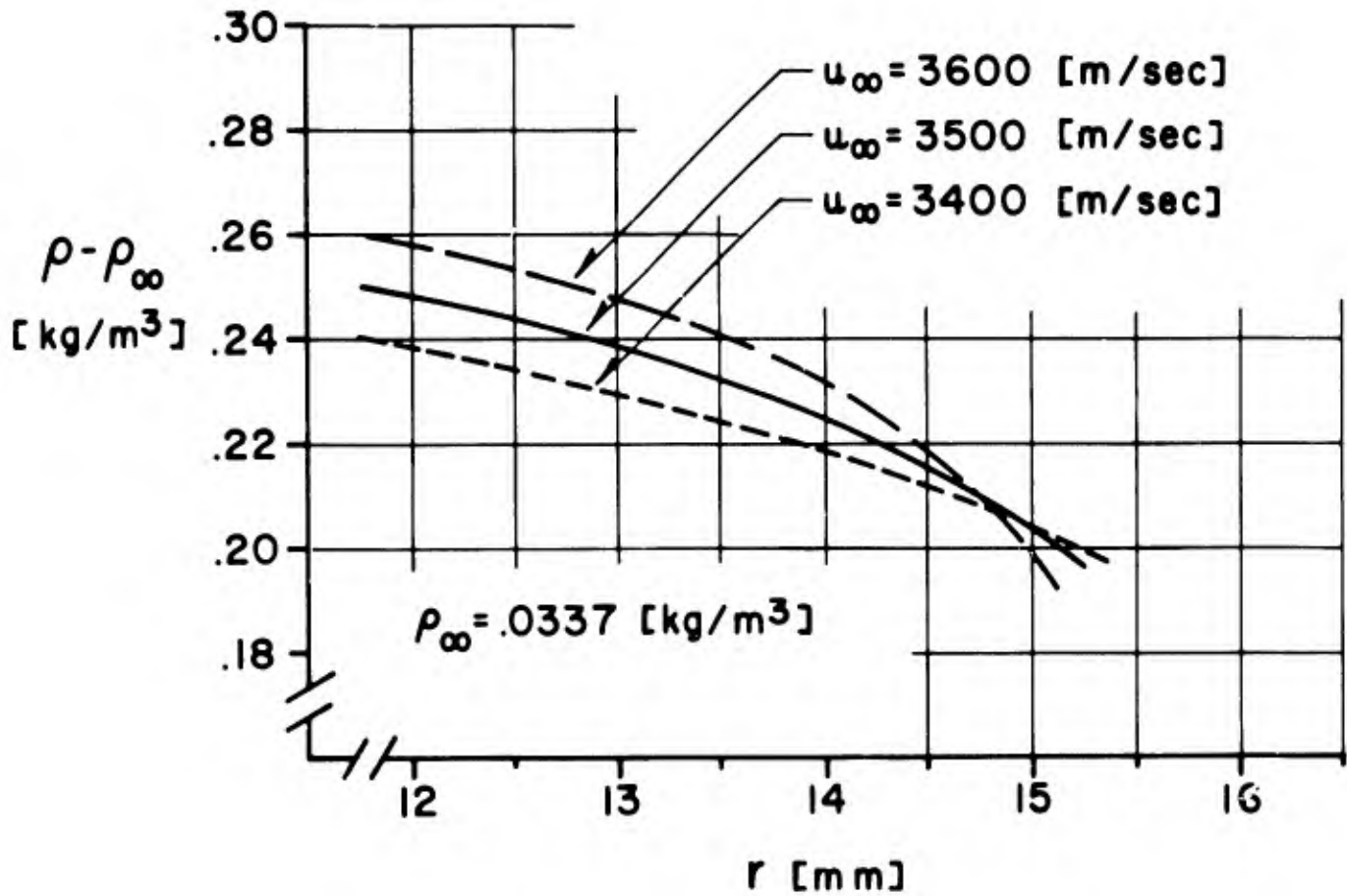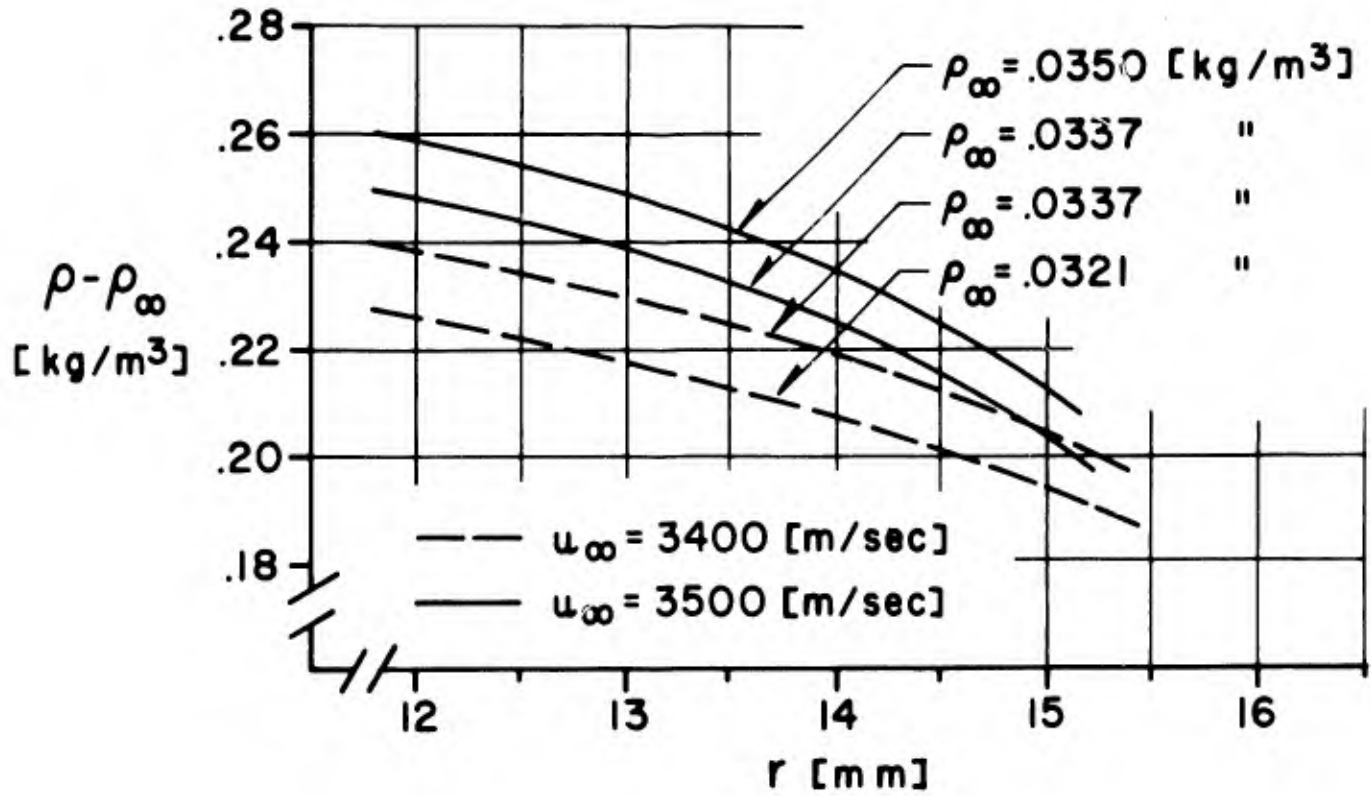
Figure 6. Theoretical Density Distribution, $\rho - \rho_\infty$ Versus r, Across the Shock Layer for Different Free Stream Density ρ_∞ and Free Stream Velocity u_∞
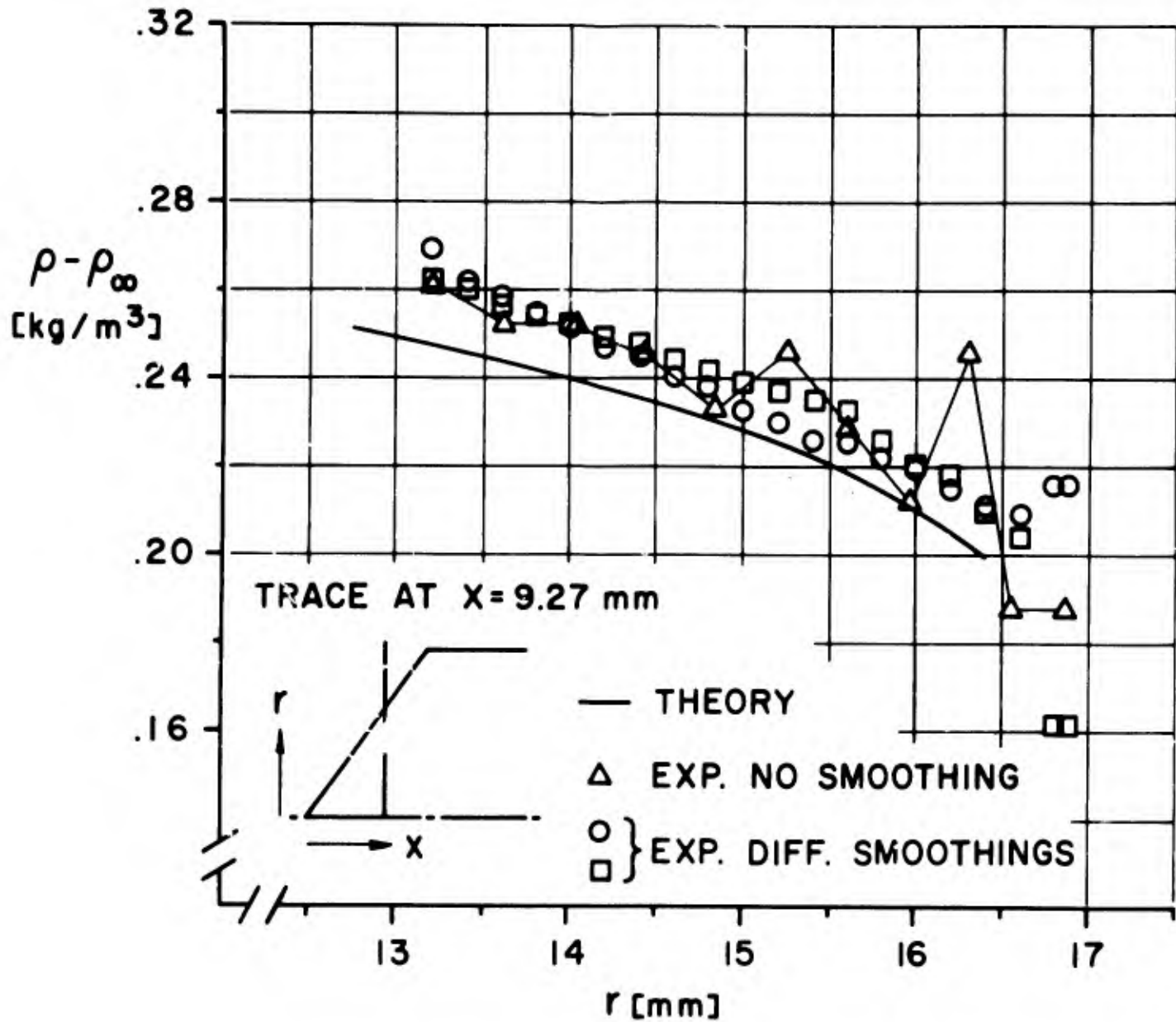
Figure 7. Density Distribution, $\rho - \rho_\infty$ Versus r, Across the Shock Layer Illustrating the Effect of Smoothing the Fringe Shift Data. Shown also is the Theoretical Distribution Based on $u_\infty = 3500$ [m/sec], $T_{\infty 2} = 388.5$ [°K] $\rho_\infty = 0.0337$ [kg/m^3], $\rho_\infty = 0.34 \times 10^5$ [d/cm^2]

22
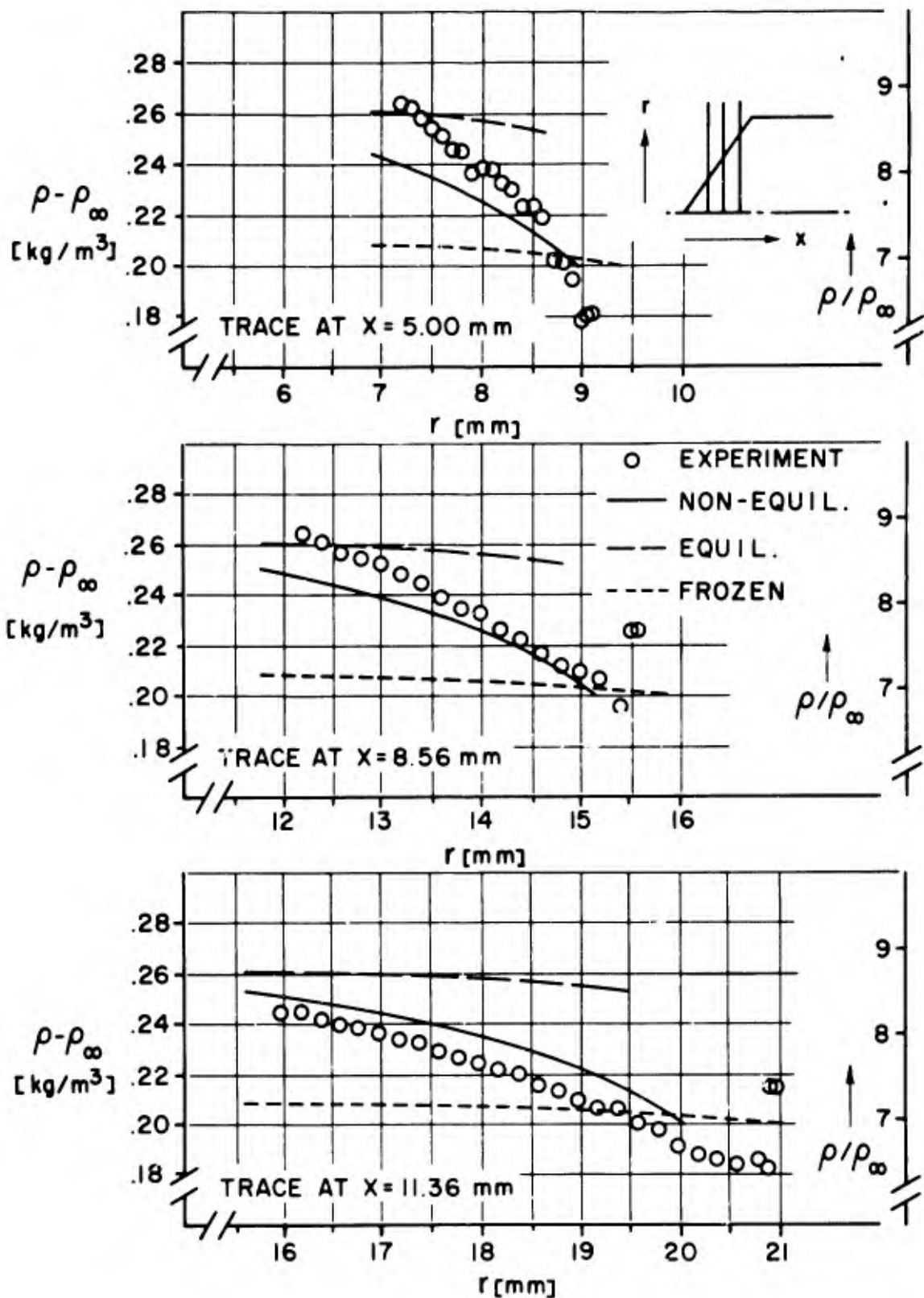
Figure 8. Comparison Between Experimental and Theoretical Density Distributions, $\rho - \rho_\infty$ Versus r, Across the Shock Layer at Three Traces. Theoretical Curves are Computed for Chemical Nonequilibrium Flow, Chemical Equilibrium Flow and Chemically Frozen Flow. Vibrational Equilibrium is Assumed for all Three Cases. Theory Based on u_∞ = 3500 $[m/sec]$, T = 388.5 $[^\circ K]$, ρ_∞ = 0.0337 $[kg/m^3]$ p_∞ = 0.34 x 10^5 $[d/cm^2]$

distribution obtained from the smoothed data curve quite well. Note the effect which the different smoothings and deshocking constants have on the spurious density values near the shock.

In Figure 8, three typical experimental density traces are compared with theoretical density traces for (1) vibrational equilibrium, frozen dissociation flow; (2) vibrational equilibrium, dissociation nonequilibrium flow; and (3) equilibrium flow. With the range of density from 0 to 0.16 kg/m^3 suppressed in the figures, the density distribution for calorically perfect (completely frozen) gas would be just below the abscissa. The experimental traces are in good agreement with the theoretical prediction for nonequilibrium flow, though the theoretical values are typically low near the tip and high near the shoulder of the cone in relation to the experimental data. This behavior is confirmed by the other traces also. The density trace in Figure 9 illustrates the effect of the different refractivities of molecular oxygen as reported in Reference 12 and Reference 13, respectively.

Figure 10 shows the experimental and theoretical isopycnal lines ρ/ρ_∞ = constant. All 10 traces were used in drawing these isopycnals without further smoothing of the data.

In Figure 11, the experimental shock geometry is compared with theoretical predictions. The relative large difference between the shock angle for calorically perfect gas, (in terms of relaxation times $\tau_V \to \infty$, $\tau_D \to \infty$), and the gas in the vibrational equilibrium, frozen dissociation state, ($\tau_V = 0$, $\tau_D \to \infty$), is made plausible by the large amount of energy which is stored in the vibrational mode. The vibrational energy is about 12 percent of the total enthalpy and comparable to the enthalpy of dissociation for the conditions of the experiment. The noticeable difference between the experimental and the theoretical shock geometry, assuming vibrational equilibrium and dissociation nonequilibrium flow, is probably caused by two effects:

(1) The enthalpy is expected to be higher than indicated by the free stream translational temperature. The total enthalpy could be increased as much as 2.8 percent by vibrational energy which is frozen out
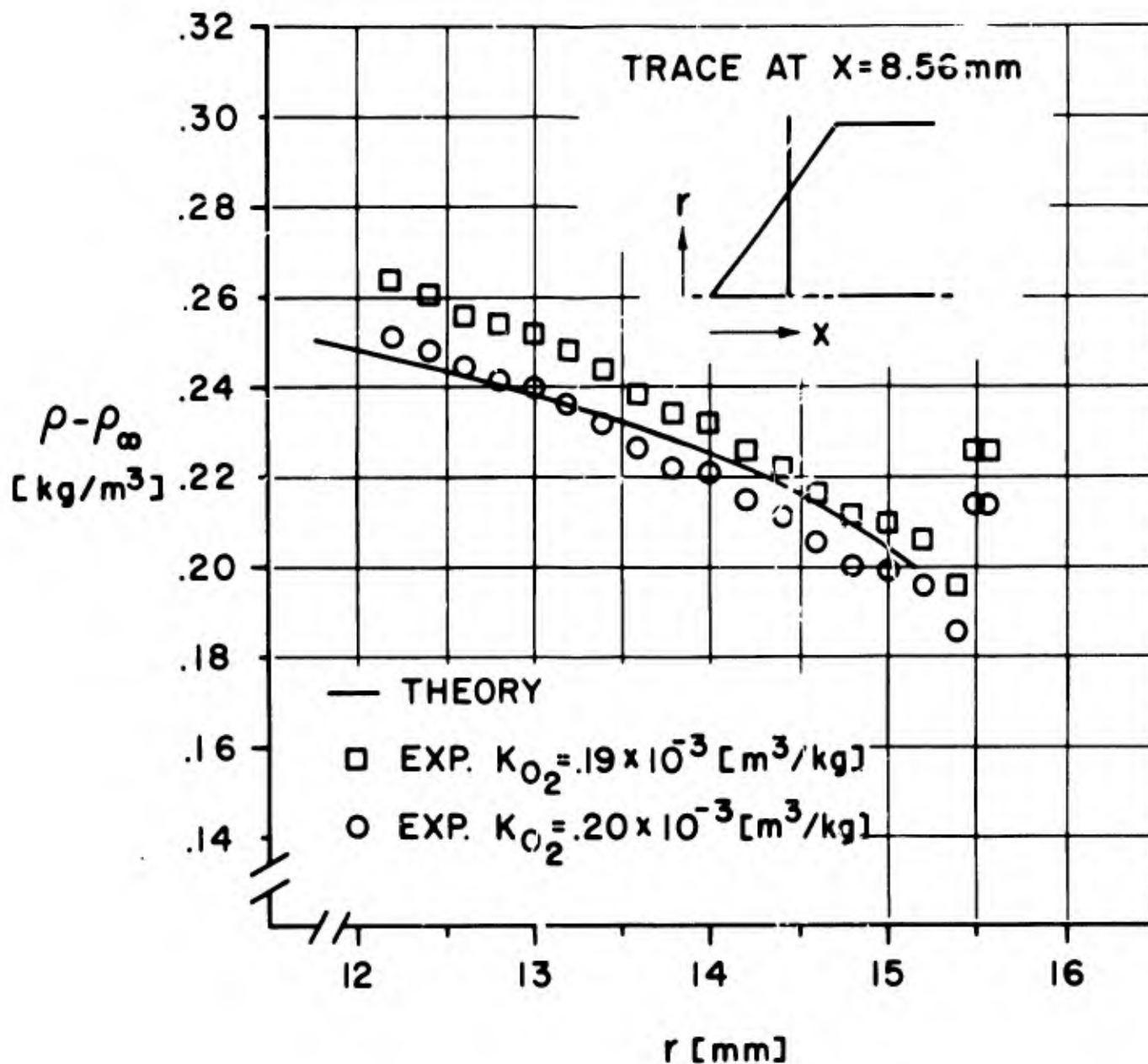
Figure 9. Experimental and Theoretical Density Distributions. Experimental Distribution Calculated for Different Values of the Index of Refraction for Molecular Oxygen
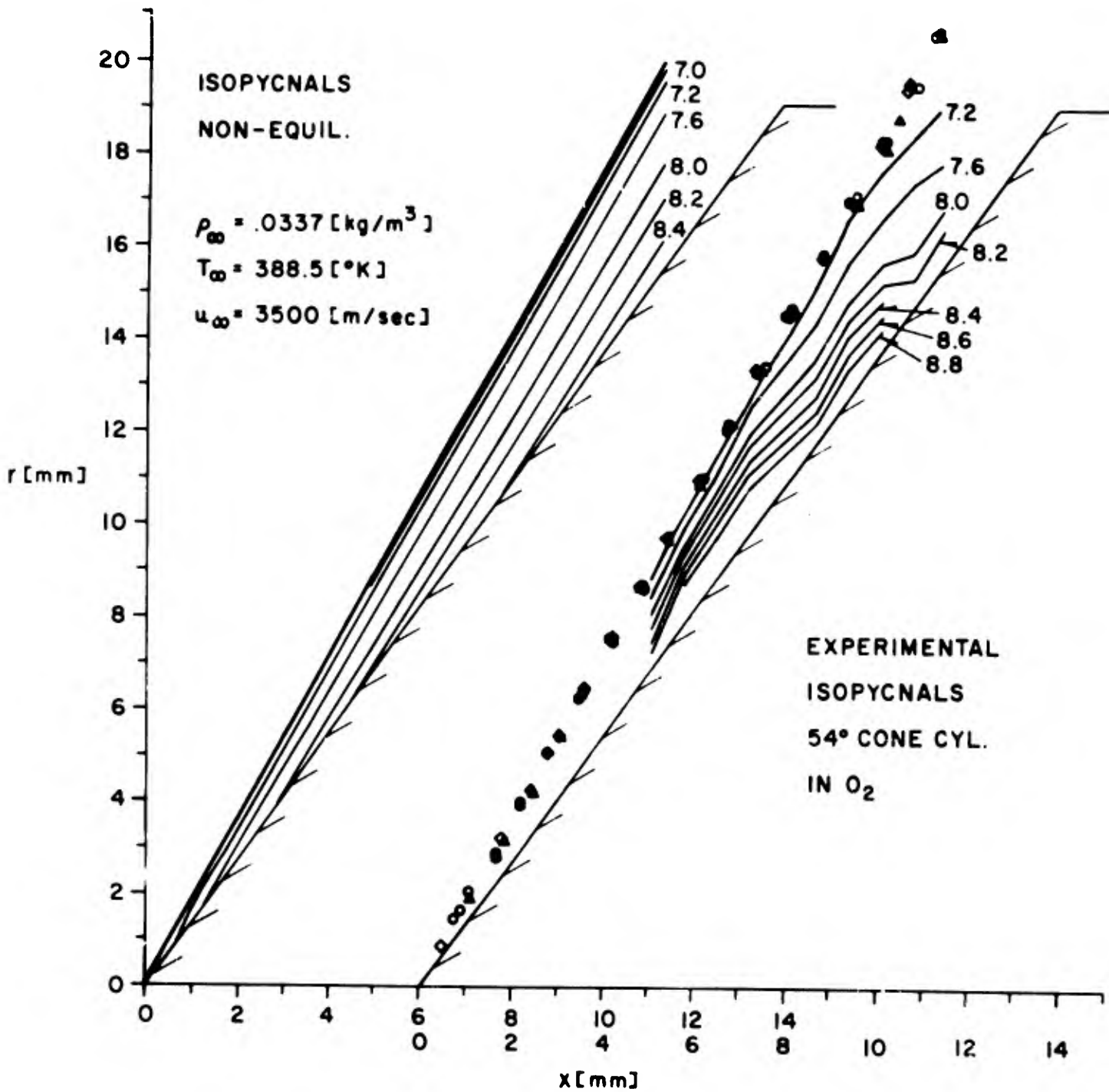
25

Figure 10.   Experimental and Theoretical Isopycnals, Lines of Constant
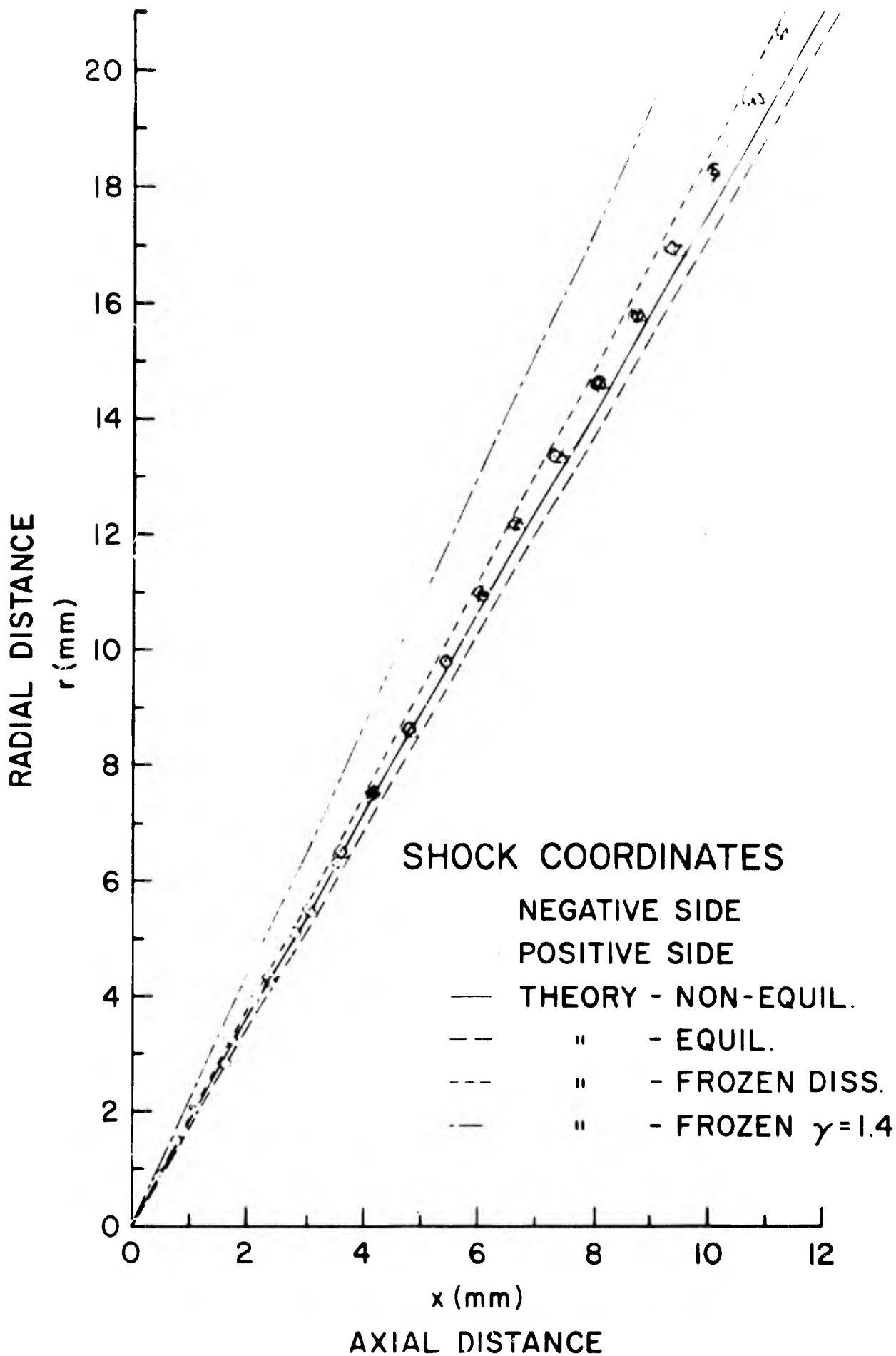Density Ratio ρ/ρ_∞

26

Figure 11. Experimental and Theoretical Shock Geometry

27

in the rapid unsteady expansion of the test gas. The additional energy has not been accounted for in the computation for nonequilibrium flow, but is expected to cause an increase in the shock angle. Representative calculations for con cal flow with frozen chemistry give an increase of 0.5 degree in shock angle.

(2) Although the assumption of vibrational equilibrium throughout the shock layer appears to be satisfactory for a ratio of relaxation times $\tau_D/\tau_V \sim 50$, where τ_D is defined[18] as $1/\tau_D = k_{O_2} (n_{O_2}/N_O)$ with n_{O_2} number of oxygen molecules/cc, and N_O Avogadro's number, this assumption most likely will affect the shock geometry. Numerical calculations [19-21] show that the inclusion of vibrational relaxation will increase the shock angle and/or standoff distance. For conditions where coupling between vibration and dissociation relaxation is important, the change in shock geometry is appreciable.

Actually, inspection of the frame interferogram in Figure 2 suggests the presence of a thin vibrational relaxation layer. The experimental observation of this layer is surprising, in view of the large effect of impurities in producing vibrational relaxation. The "break" in the fringes, which is observed close to the shock (better visible in the upper portion of the interferogram), indicates the end of the vibrational relaxation layer, or the beginning of the dissociation relaxation layer. With the vibrational mode relaxing much faster than the dissociation mode, an abrupt change of fringe slope results. The relaxation length along the streamline, based on the velocity behind the shock and relaxation time of Reference 22, is in good agreement with the observed length.

It may be mentioned that the displacement effect of the highly cooled boundary layer is too small to account for the difference in experimental and theoretical shock angle.

VII. CONCLUSIONS

Experimental density distributions in the shock layer of a non-equilibrium flow field are presented. The accuracy of the data is

28

determined by about five percent error in the fringe shift measurement and, at most, five percent error in the reduction process. Additional error may be introduced by the uncertainty in the index of refraction for molecular oxygen at higher temperatures. It is important to note that the random scatter of the raw unsmoothed data points is less than three percent of the fringe shift for most of the field. There is no evidence of large nonuniformities in the shock layer flow. These points are emphasized in view of the experimental apparatus used for generating the test flow. The major uncertainty lies in the free stream conditions which, however, do not sensitively affect the data in the shock layer.

Within the range of possible free stream conditions the theoretical predictions, using the simplified gas model described earlier and rate coefficients available in the literature, are in good agreement with the experimental data.

ACKNOWLEDGMENTS

J. H. SPURK   J. M. BARTOS

REFERENCES

1. Trimpi, R. L. NASA TR R-133 (1962).

2. Trimpi, R. L. and Callis, L. B. NASA TR R-223 (1965).

3. Stoddard, F. J.; Hertzberg, A. and Hall, J.G. Fourth Hypervelocity Techniques Symposium (Arnold Air Force Station, Tennessee, 1965), 145-171.

4. Spurk, J. H. and Shear, D. D. Phys. Fluids 8, 1913-1915 (1965).

5. Spurk, J. H. Fourth Hypervelocity Techniques Symposium (Arnold Air Force Station, Tennessee, 1965), 111-144.

6. Jones, J. J. Fourth Hypervelocity Techniques Symposium (Arnold Air Force Station, Tennessee, 1965), 7-26.

7. Givens, J. J.; Page, W. A. and Reynolds, R. M. Fourth Hypervelocity Techniques Symposium (Arnold Air Force Station, Tennessee, 1965), 27-48.

8. Norfleet, G. D.; Lacey, J. J., Jr. and Whitfield, J. D. Fourth Hypervelocity Techniques Symposium (Arnold Air Force Station, Tennessee, 1965), 49-110.

9. Mathews, D. C. Phys. Fluids 2, 170-178 (1959).

10. Bennett, F. D.; Carter, W. C., and Bergdolt, V. E. J. Appl. Phys. 23, 453-469 (1952).

11. Ladenberg, R. and Bershader, D. High Speed Aerodynamics and Jet Propulsion (Princeton University Press, Princeton, N.J.), Vol. IX, Sect. A3, 47-78 (1954).

12. Alpher, R. A. and White, D. R. Phys. Fluids 2, 153-161 (1959).

13. Anderson, J. H. B. UTIAS Annual Progress Report (1965) 832-833.

14. Spurk, J. H.; Gerber, N. and Sedney, R. Aberdeen Proving Ground BRL Report No. 1276 (1965).

15. Wray, K. L. Hypersonic Flow Research (F. R. Riddell, Ed., Academic Press, N. Y. 1962) 181-204.

16. Hall, J. G.; Eschenroeder, A. Q. and Marrone, P. V. CAL Report No. AF1413-A-2 (1962).

17. Roshko, A. Phys. Fluids 3, 835-842 (1960).

18. Wray, K. L. J. Chem. Phys. $\underline{37}$, 1254-1263 (1962).

19. Springfield, J. F. Proceedings of the 1964 Heat Transfer and Fluid Mechanics Institute (W. H. Giedt and S. Levy, Eds., Stanford University Press 1964) 182-197.

20. Marrone, P. V. CAL Rep. No. QM-1626-A-12(1) (1963).

21. DeJarnette, F. R. Doctoral Thesis, Virginia Polytechnic Institute (1965).

22. Camac, M. J. Chem. Phys. $\underline{34}$, 448-459 (1961).

DOCUMENT CONTROL DATA - R&D

(Security classification of title, body of abstract and indexing annotation must be entered when the overall report is classified)

1 ORIGINATING ACTIVITY (Corporate author)	2a REPORT SECURITY CLASSIFICATION
US Army Ballistic Research Laboratories Aberdeen Proving Ground, Maryland	Unclassified
	2b GROUP

3 REPORT TITLE

INTERFEROMETRIC MEASUREMENT OF THE NONEQUILIBRIUM FLOW FIELD AROUND A CONE

4 DESCRIPTIVE NOTES (Type of report and inclusive dates)

5 AUTHOR(S) (Last name, first name, initial)

Spurk, Joseph H. and Bartos, Joan M.

6 REPORT DATE	7a TOTAL NO OF PAGES	7b NO OF REFS
August 1966	36	22

8a CONTRACT OR GRANT NO.	9a ORIGINATOR'S REPORT NUMBER(S)
b. PROJECT NO RDT&E 1P222901A201	Report No. 1333
c	9b OTHER REPORT NO(S) (Any other numbers that may be assigned this report)
d	

10 AVAILABILITY/LIMITATION NOTICES

Distribution of this document is unlimited.

11 SUPPLEMENTARY NOTES	12 SPONSORING MILITARY ACTIVITY
	US Army Materiel Command Washington, D. C.

13 ABSTRACT

Interferometric measurement of the density field around a cone in a stream of oxygen at approximately 10,000 ft/sec is reported. The test flow was generated in an expansion tube, which utilizes an unsteady expansion for the purpose of total enthalpy multiplication. The experiment shows that vibrational equilibrium is achieved close behind the shock, while chemical relaxation occurs throughout the shock layer. The experimental density distribution and shock shape are compared with theoretical predictions, and good agreement is found.

DD FORM 1473 , 1 JAN 64

14 KEY WORDS	LINK A		LINK B		LINK C	
	ROLE	WT	ROLE	WT	ROLE	WT
High Enthalpy Flow Nonequilibrium Flow Interferometry Chemical Reactions						

INSTRUCTIONS

1. **ORIGINATING ACTIVITY:** Enter the name and address of the contractor, subcontractor, grantee, Department of Defense activity or other organization *(corporate author)* issuing the report.

2a. **REPORT SECURITY CLASSIFICATION:** Enter the over-all security classification of the report. Indicate whether "Restricted Data" is included. Marking is to be in accordance with appropriate security regulations.

2b. **GROUP:** Automatic downgrading is specified in DoD Directive 5200.10 and Armed Forces Industrial Manual. Enter the group number. Also, when applicable, show that optional markings have been used for Group 3 and Group 4 as authorized.

3. **REPORT TITLE:** Enter the complete report title in all capital letters. Titles in all cases should be unclassified. If a meaningful title cannot be selected without classification, show title classification in all capitals in parenthesis immediately following the title.

4. **DESCRIPTIVE NOTES:** If appropriate, enter the type of report, e.g., interim, progress, summary, annual, or final. Give the inclusive dates when a specific reporting period is covered.

5. **AUTHOR(S):** Enter the name(s) of author(s) as shown on or in the report. Enter last name, first name, middle initial. If military, show rank and branch of service. The name of the principal author is an absolute minimum requirement.

6. **REPORT DATE:** Enter the date of the report as day, month, year; or month, year. If more than one date appears on the report, use date of publication.

7a. **TOTAL NUMBER OF PAGES:** The total page count should follow normal pagination procedures, i.e., enter the number of pages containing information.

7b. **NUMBER OF REFERENCES:** Enter the total number of references cited in the report.

8a. **CONTRACT OR GRANT NUMBER:** If appropriate, enter the applicable number of the contract or grant under which the report was written.

8b, 8c, & 8d. **PROJECT NUMBER:** Enter the appropriate military department identification, such as project number, subproject number, system numbers, task number, etc.

9a. **ORIGINATOR'S REPORT NUMBER(S):** Enter the official report number by which the document will be identified and controlled by the originating activity. This number must be unique to this report.

9b. **OTHER REPORT NUMBER(S):** If the report has been assigned any other report numbers *(either by the originator or by the sponsor)*, also enter this number(s).

10. **AVAILABILITY/LIMITATION NOTICES:** Enter any limitations on further dissemination of the report, other than those imposed by security classification, using standard statements such as:

  (1) "Qualified requesters may obtain copies of this report from DDC."

  (2) "Foreign announcement and dissemination of this report by DDC is not authorized."

  (3) "U. S. Government agencies may obtain copies of this report directly from DDC. Other qualified DDC users shall request through

                                            ."

  (4) "U. S. military agencies may obtain copies of this report directly from DDC. Other qualified users shall request through

                                            ."

  (5) "All distribution of this report is controlled. Qualified DDC users shall request through

                                            ."

If the report has been furnished to the Office of Technical Services, Department of Commerce, for sale to the public, indicate this fact and enter the price, if known.

11. **SUPPLEMENTARY NOTES:** Use for additional explanatory notes.

12. **SPONSORING MILITARY ACTIVITY:** Enter the name of the departmental project office or laboratory sponsoring *(paying for)* the research and development. Include address.

13. **ABSTRACT:** Enter an abstract giving a brief and factual summary of the document indicative of the report, even though it may also appear elsewhere in the body of the technical report. If additional space is required, a continuation sheet shall be attached.

It is highly desirable that the abstract of classified reports be unclassified. Each paragraph of the abstract shall end with an indication of the military security classification of the information in the paragraph, represented as *(TS)*, *(S)*, *(C)*, or *(U)*.

There is no limitation on the length of the abstract. However, the suggested length is from 150 to 225 words.

14. **KEY WORDS:** Key words are technically meaningful terms or short phrases that characterize a report and may be used as index entries for cataloging the report. Key words must be selected so that no security classification is required. Identifiers, such as equipment model designation, trade name, military project code name, geographic location, may be used as key words but will be followed by an indication of technical context. The assignment of links, rules, and weights is optional.